A Systematic Study of Vinyl ether-based Poly(ethylene oxide) Side Chain Polymer Electrolytes

Andreas J. Butzelaar[a], Kun L. Liu[b], Philipp Röring[b], Gunther Brunklaus[b,c], Martin Winter[b,c], Patrick Theato[a,d]*

a) Karlsruhe Institute of Technology (KIT), Institute for Chemical Technology and Polymer Chemistry (ITCP), Engesserstraße 18, 76131 Karlsruhe, Germany.

b) Helmholtz-Institute Münster, IEK-12, Forschungszentrum Jülich GmbH, Corrensstraße 46, 48149, Münster, Germany.

c) MEET Battery Research Center / Institute of Physical Chemistry, University of Münster, Corrensstraße 46, 48149 Münster, Germany.

d) Karlsruhe Institute of Technology (KIT), Soft Matter Laboratory - Institute for Biological Interfaces III (IBG-3), Hermann-von-Helmholtz-Platz 1, 76344 Eggenstein-Leopoldshafen, Germany.

KEYWORDS: Polymer Electrolyte; PEO architectures; Vinyl ether with PEO side chains; 'Grafting-to'; Thermal and electrochemical properties; Li^+ conductivity

Abstract: Herein we report on the synthesis of a systematic library of vinyl ether-based poly(ethylene oxide) PEO side chain copolymers in order to reduce crystallization of PEO. The influence of different grafted PEO side chain lengths, the grafting density and the $[Li^+]$:[EO] ratio after mixing with LiTFSI on the *glass transition temperature* (T_g), the crystallinity and the resulting ionic conductivity was examined. Copolymers bearing longer PEO side chains and higher grafting densities show higher crystallization tendencies while their T_g is reduced at the same time. Furthermore, the addition of LiTFSI reduces the crystallization, but increases the T_g. Since these effects are directly impacting the ionic conductivity, we demonstrate that the different parameters need to be carefully adjusted in order to balance their influence. In this way, a fundamental view enlightening PEO side chain copolymers for their application as polymer electrolytes is provided.

1. Introduction

The introduction of the first rechargeable lithium-ion battery (LIB) by Sony Corporation in 1991 enabled their commercialization and exploitation in numerous technical applications such as portable electronic devices and electric vehicles.[1] Nearly 30 years later, the battery sector is still constantly growing due to an expanding demand in rechargeable batteries and extensive

research in this area.[2] Currently, commercially available LIBs employ liquid organic solvents as electrolytes. However, *organic liquid electrolytes* have significant drawbacks since they are in most cases toxic, volatile, and flammable,[3,4] eventually resulting in fire or explosion in case of mechanical, thermal, or electrical impact.[5] In contrast, *solid-state electrolytes* (SSEs) are beneficial in terms of mechanical strength, toxicity, electrochemical stability and thermal tolerance, thus potentially eliminating the safety issues of *organic liquid electrolyte*-based batteries.[6] SSE materials in principle can be divided into *inorganic solid electrolytes* and *polymer electrolytes* (PEs*)*, the latter further categorized into *solid polymer electrolytes* (SPE) and *gel polymer electrolytes* (GPE).[7] In polymer electrolytes, the ions diffuse in general in the space provided by the free volume of the polymer, meaning that conductivity is only possible above the *glass transition temperature* (T_g) of the polymer.[8,9]

Even though many polymer electrolytes have been introduced,[10–12] poly(ethylene oxide) (PEO) as ion conducting matrix for alkali metal salts[13] is among the most utilized polymer electrolytes for which extensive studies have been conducted.[14–17] PEO affords a good chain flexibility, low *glass transition temperature* (T_g), remarkable electrochemical stability against lithium metal, and great solubility for conductive lithium salts, but it still suffers from low ionic conductivities of 10^{-5} to 10^{-1} mS cm^{-1} at temperatures below its melting point (~65°C).[18] Nevertheless, its potential for solid state battery application in electric vehicles was successfully demonstrated by Bolloré,[19] introducing the Lithium Metal Polymer (LMP) battery technology to the markets in 2011, and to date, more than 8000 vehicles are operated based on the LMP technology, illustrating that PEO and variants thereof are not only of contemporary interest but also practically extremely relevant.[20,21]

To improve the ionic conductivity of PEO, its inherent crystallization can be reduced by different approaches such as the addition of plasticizer,[22,23] nanofillers,[24] blending with other polymers[25] or by crosslinking.[26,27] One additional approach comprises the synthesis of polymers bearing grafted PEO side chains. Because of being anchored to the backbone chain, the

crystallization of the PEO side chains is reduced resulting in superior ionic conductivity at lower temperatures.[28]

In 2016, Itoh et al.[29] described the ionic conductivity of pure vinyl ether-based ethylene oxide side chain homopolymers with $(O\text{-}CH_2\text{-}CH_2)_n$ side chain lengths of n = 3, 6, 10 and 23.5 units, corresponding to a side chain molecular weight of ~ 160, 300, 470 and 1000 g mol^{-1} respectively. They found the highest ionic conductivity when using LiTFSI with a ratio of [Li^+]:[EO] 1:20 and the longest side chain (23.5 units/1000 g mol^{-1}) at temperatures above 20 °C. However, the majority of their employed side chains were relatively short (10 units or less), and they did not use a PEO side chain longer than 23.5 units (1000 g mol^{-1}), although their findings show a clear trend that longer side chains might be beneficial above room temperature. In addition, to best of our knowledge, there is no report of the impact of the grafting density of such vinyl ether-based PEO side chain PEs on the achievable electrochemical properties.

Therefore, we expand the area of vinyl ether-based PEO side chain structures in this study in order to draw a comprehensive picture of how the different parameters such as PEO side chain length, LiTFSI content and grafting density influence the thermal properties as well as the ionic conductivity of those PEs. This will provide an important and fundamental understanding of the structure-property relationship that is valuable for various PEO side chain polymer electrolytes, independent of the nature of their polymer main chain backbone.

2. Experimental Section

2.1 Materials

Isobutyl vinyl ether (IBVE, 99%, Aldrich), acetic acid (100%, CarlRoth), diethylene glycol vinyl ether (98%, TCI), *p*-toluenesulfonyl chloride (99%, Aldrich), triethylamine (99%, Aldrich), 2,6-di-*tert*-butylpyridine (DtBP, > 97%, Aldrich), ethylaluminum sesquichloride (0.4 M in hexane, Acros Organics), sodium hydride (60 % dispersion in mineral oil, Aldrich),

poly(ethylene oxide) monomethyl ether (M_n ~ 400, 550, 1000, 2000, TCI), poly(ethylene oxide) monomethyl ether (M_n ~ 750, Aldrich), were used as received. Cyclohexyl vinyl ether (> 98%, TCI) was filtered through activated basic alumina prior to use. Bis(trifluoromethane)sulfonimide lithium salt (LiTFSI, 99.95%, Aldrich) was dried at 80 °C under vacuum for 2 days and subsequently stored inside a glove box (MBraun Unilab, < 0.1 ppm H_2O, < 0.1 ppm O_2) under inert argon atmosphere. The adduct of IBVE and acetic acid (i.e. the cationogen) was synthesized as described in literature.[30] All other solvents and reagents were of analytical grade or higher and were used without further purification.

2.2 Synthesis of diethylene glycol vinyl ether tosylate (2)

Diethylene glycol vinyl ether (4.84 g, 36.6 mmol, 1.00 eq.) and triethylamine (4.07 g, 40.3 mmol, 1.1 eq.) were given into a round-bottom flask and taken up with 50 mL of dichloromethane (DCM). The reaction mixture was cooled to 0 °C and while tosyl chloride (7.33 g, 38.5 mmol, 1.05 eq.) was added under stirring. After 1 hour, the ice bath was removed, and the reaction mixture was stirred for additionally 20 hours before it was stopped. The solution was washed twice with 1 M $HCl_{(aq.)}$, once with 1 M $NaOH_{(aq.)}$ and once with pure water. The combined aqueous phases were extracted twice with DCM. The combined organic phases were then dried over $CaCO_3$/$MgSO_4$, filtered, and the solvent was removed under reduced pressure yielding a slightly yellow oil. Subsequently, the crude product was purified by column chromatography using DCM:petrol ether in a ratio of 3:1. The obtained product was dried over CaH_2 and filtered through basic alumina to yield 4.51 g (81%) of a colorless oil.

^{1}H NMR (400 MHz, DMSO-d_6) δ 7.78 (d, J = 8.4 Hz, 2H), 7.48 (d, J = 8.1 Hz, 2H), 6.47 (dd, J = 14.3, 6.8 Hz, 1H), 4.16 (dd, J = 14.3, 1.8 Hz, 1H), 4.12 (t, J = 4.4 Hz, 2H), 3.97 (dd, J = 6.8, 1.8 Hz, 1H), 3.70 (t, J = 5.0, 4.4 Hz, 2H), 3.59 (t, J = 4.2 Hz, 2H), 3.54 (t, J = 4.9, 4.4 Hz, 2H), 2.42 (s, 3H).
^{13}C NMR (101 MHz, DMSO-d_6) δ 151.79, 144.89, 132.38, 130.12, 127.62, 86.93, 69.92, 68.74, 67.90, 67.08, 21.09.

2.3 Synthesis of precursor polymer A/B

Cyclohexyl vinyl ether (**A**: 8.81 g, 69.84 mmol, 100.00 eq.; **B**: 1.76 g, 13.96 mmol, 60.00 eq.), diethylene glycol vinyl ether tosylate (5.00 g, 17.46 mmol, 25.00 eq.; **B**: 4.00 g, 13.96 mmol, 60.00 eq.), the cationogen (**A**: 0.112 g, 0.70 mmol, 1.00 eq.; **B**: 0.037 g, 0.23 mmol; 1.00 eq.), THF (**A**: 2.52 g, 2.83 mL, 34.92 mmol, 50.00 eq.; **B**: 0.839 g, 0.944 mL, 11.64 mmol, 50.00 eq.), DtBP (**A**: 0.668 g, 3.49 mmol, 5.00 eq.; **B**: 0.222 g, 3.49 mmol, 5.00 eq.) and **A**: 100 mL/**B**: 30 mL of dry toluene were mixed in a pre-dried round-bottom flask and closed air-tight. Subsequently, the flask was placed in an ice bath and the polymerization was started *via* addition of $Et_3Al_2Cl_3$ (**A**: 0.864 g, 3.49 mmol, 5.00 eq.; as 0.4 M solution in 8.73 mL of *n*-hexane; **B**: 0.288 g, 1.16 mmol, 5.00 eq.; as 0.4 M solution in 2.91 mL of *n*-hexane). After 2 hours the reaction was quenched by addition of 10 mL of a 1% NH_4OH in MeOH solution. Subsequently, most of the methanol was removed under reduced pressure and ethyl acetate and brine were added to separate the phases. The organic phase was washed three times with 1 m $HCl_{(aq)}$ and the combined aqueous phase was extracted once with EtOAc. The combined organic phases were dried over $MgSO_4$, filtered and most of the solvent was removed. Then, the polymer was further purified by precipitating three times from THF into MeOH. Subsequently, the resulting white solid was dried at 40 °C under vacuum overnight. Yield: **A**: 10.8 g (78%)/**B**: 4.3 g (79%)

^{1}H NMR (400 MHz, Chloroform-d) δ 7.87 – 7.69 (m, 2H, $\mathbf{H}_{arom.}$ tosyl), 7.38 – 7.28 (m, 2H, $\mathbf{H}_{arom.}$ tosyl), 4.25 – 3.98 (m, 2H, $OCH_2C\mathbf{H}_2$tosyl), 3.70 – 3.37 (m, XH, C**H** backbone + $C\mathbf{H}_2$ ethylene oxide), 3.37 – 3.18 (m, YH, C**H** cyclohexyl), 2.52 – 2.37 (m, 3H, $C\mathbf{H}_3$ tosyl), 2.01 – 0.94 (m, ZH, $C\mathbf{H}_2$ backbone + $C\mathbf{H}_2$ cyclohexyl).
A: X = 11, Y = 4, Z = 50; **B**: X = 8, Y = 1, Z = 14

A: **SEC** M_n = 21200 g mol^{-1} $Đ$ = 1.43; **B**: **SEC** M_n = 17200 g mol^{-1} $Đ$ = 1.52

2.4 Synthesis of PEO side chain copolymers A/B

General procedure: Sodium hydride (60% dispersion in mineral oil, 3.2 eq. in respect to tosyl groups in the **precursor** copolymer **A**/**B**, final concentration = 0.134 mol L^{-1}) was placed into a round-bottom flask and the atmosphere was changed to N_2, before being suspended in

dry tetrahydrofuran (THF). While stirring, poly(ethylene oxide) monomethyl ether (mPEOz); z = 400, 550, 750, 1000, 2000; 3.00 eq., final concentration = 0.126 mol L^{-1}) dissolved in dry THF was slowly added. After the H_2 formation stopped (~ 30 min), the **precursor** copolymer **A**/**B** (1.00 eq., final concentration = 0.042 mol L^{-1}) in THF was added and the reaction mixture was heated to 40 °C and stirred for 24 hours. The reaction was stopped by addition of H_2O and the solvent was removed under reduced pressure. Subsequently, the remaining crude mixture was taken up in a small amount of methanol and dialyzed against methanol to remove the excess of mPEOz. Spectra/Por™ 6 dialysis tubing with a molecular weight cut-off (MWCO) of 2 kD was used for the removal of mPEOz = 400, 550 and 750, 3.5 kD for the removal of mPEO1000 and 8 kD for the removal of mPEO2000, respectively. After the completed dialysis, the solvent was removed under reduced pressure and the resulting polymer was dried at 40 °C under vacuum overnight. Typical yields 60-80%. More details can be found in **Table S1/2**.

2.5 Polymer electrolyte (PE) preparation

Prior to the PE preparation, the respective polymer was dried at 80 °C under vacuum overnight. The polymer as well as the corresponding amount of LiTFSI with predefined ratios of $[Li^+]$:[EO] 1:5, 1:10, 1:15 or 1:20 were both dissolved in acetone. Subsequently, both solutions were combined to yield a homogenous mixture. Acetone was removed slowly under reduced pressure at 50 °C, followed by drying the polymer electrolytes under reduced pressure (10^{-3} mbar) and 80 °C for 24 hours.

2.6 Electrochemical Impedance Spectroscopy (EIS)

For EIS measurements, coin cell-type cells (CR2032) were assembled, where the previously prepared polymer electrolytes were sandwiched between two stainless steel electrodes using a Mylar foil spacer ring (thickness l = 100 µm, inner diameter = 8 mm) Subsequently, these cells were preconditioned in a temperature chamber (Binder MK53, controlled with the Autolab Software Nova 2.1.3) with a gradual increase of temperature from 20 °C – 70 °C in 10 °C steps while maintaining each temperature for 2 h. 1 h after the preconditioning was finished,

measurements were carried out by gradually increasing the temperature in 10 °C steps from 0 °C to 70 °C with each temperature being maintained for 2 h to attain a thermal equilibrium. The measurements were performed using a PGSTAT302N potentiostat/galvanostat (Autolab) over a frequency range of 1 MHz – 1 Hz with an amplitude of 10 mV. The ionic conductivity σ was calculated according to the following equation: $\sigma = (1/R_b) \cdot (l\ A^{-1})$; R_b being the bulk resistance that can be accessed from the Nyquist plot (**Figure S7**), l is the film thickness (l = 100 µm) and A is the film area ($A = 5.03 \bullet 10^{-5}$ m^2). For each PE three coin cells were prepared and measured. Subsequently, the mean average ionic conductivity of these three measurements was derived and discussed.

2.7 Thermal Gravimetric Analysis (TGA)

Thermal Gravimetric Analysis (TGA) was carried out by a TGA 5500 (TA Instruments) at a heating rate of 10 K min^{-1} under nitrogen atmosphere up to 800 °C.

2.8 Differential scanning calorimetry (DSC)

Differential scanning calorimetry was conducted on a DSC Q200 (TA Instruments) in a range from -75 °C to 70 °C with a scan rate of 5 K min^{-1} for all measurements.

2.9 Size Exclusion Chromatography (SEC)

Size exclusion chromatography was carried out in THF on a Tosoh Bioscience HLC-8320GPC EcoSEC system equipped with 3 PSS SDV columns 5 µm (100 Å, 1000 Å, 100000 Å) (8 • 300 mm), a UV and a differential refractive index (RI) detector. The operation temperature was set to 35 °C with a flow rate of 1 mL min^{-1}. The system was calibrated using poly(methyl methacrylate) (PMMA) standards ranging from 800 to 2.2 • 10^6 g mol^{-1}. Typically, 50 µL of a 2.0 mg mL^{-1} sample solution was injected onto the columns.

3. Results and Discussion

3.1 Synthesis Strategy

Based on the results of Itoh *et al.*[29] different vinyl-ether based PEO side chain copolymers were synthesized. In doing so, the focus was laid on side chain lengths above 10 repeating units (up to 54 units) since longer side chains showed promising ionic conductivities in their study. Simultaneously, a relatively low grafting density of 20% ([comonomer]:[PEO side chain] 4:1) was targeted to ensure a significant spatial distance between each PEO side chain, thus possibly suppressing crystallization.

To fulfill this goals, poly(ethylene oxide) methyl ethers (mPEOz; z is hereby defined as the corresponding average molar mass as indicated by the supplier) were used for the synthesis of a series of five different vinyl ether-based copolymers (**polymer** series **Az; z is defined as the molar mass of the corresponding mPEOz**) bearing PEO side chains *via* the 'grafting-to' approach described by Gao and Matyjaszewski.[31] For this, a precursor polymer **3** was synthesized by cationic copolymerization of cyclohexyl vinyl ether **1** and diethylene glycol vinyl ether tosylate **2**. Herein, **1** was chosen to ensure a spatial separation of the PEO chains by its bulky cyclohexyl motif while featuring comparable oxidative stability to PEO[18] (**Figure S6**). Afterwards, *post-polymerization modification* (*PPM*) employing a nucleophilic attack of *in-situ* generated mPEOz-alkoxides was conducted in order of obtaining the desired PEO side chain copolymers **4** (see **Scheme 1**).

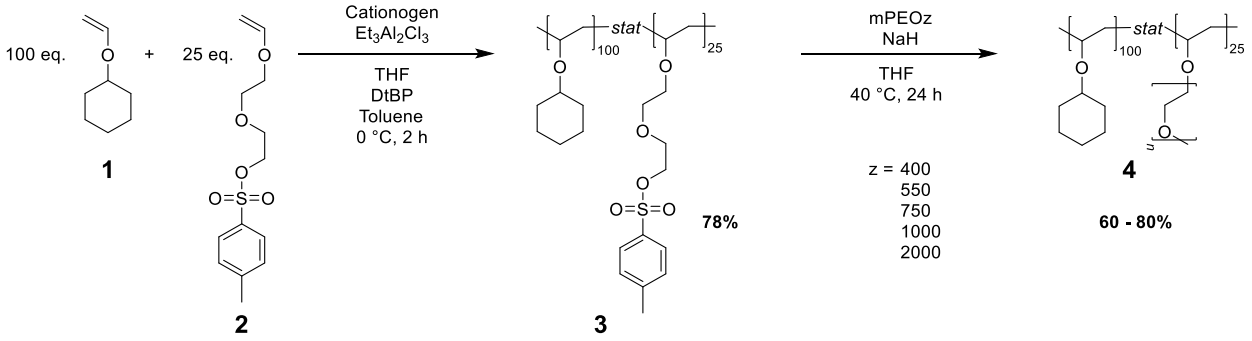

Scheme 1. Route for the synthesis of vinyl ether based PEO side chain copolymers. Starting with cyclohexyl vinyl ether (**1**) and diethylene glycol vinyl ether tosylate (**2**), a precursor polymer (**3**) was synthesized via cationic polymerization using the base-assisted initiating system[32]. Afterwards, this precursor polymer was functionalized using post-polymerization

modification via nucleophilic substitution with in-situ generated mPEO alkoxides obtaining the final polymers (**4**). All reactions featured quantitative conversions.

The successful and quantitative *PPM* was proven by SEC (**Figure 1a**, **Table S1**Fehler! Verweisquelle konnte nicht gefunden werden.) and ^{1}H NMR spectroscopy (**Figure 1b**), as well as the thermal properties, as discussed in the following.

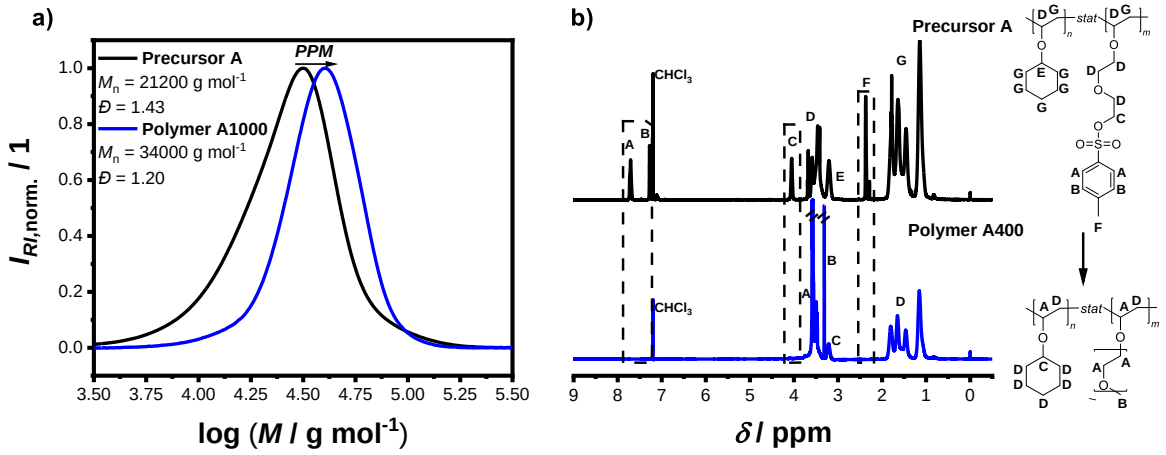

Figure 1. Successful and quantitative *post-polymerization modification* shown by **a)** SEC (exemplary **polymer A1000**) and **b)** ^{1}H NMR spectroscopy (exemplary **polymer A400**).

3.2 Thermal characterization

The thermal properties of the PEO side chain vinyl ethers were analyzed *via* DSC and TGA (summary given in **Table 1**). While the **precursor A** showed 5% weight loss (T_{d5}) at 190 °C, the functionalized PEO side chain **polymers A400 - A2000** were stable up to T_{d5} ~ 340 °C showing a good thermal stability as wells as proving once more the clean *post-polymerization modification* (**Figure S5*Fehler! Verweisquelle konnte nicht gefunden werden.***). Furthermore, the thermal stability after the addition of LiTFSI ([Li^{+}]:[EO] 1:10) was also examined, since this is more representative of the real application of these polymers. Only a negligible shift towards lower decomposition temperatures was observed, most probable because pure LiTFSI shows a lower T_d (333 °C[33]) than the pure **polymers A400 - A2000**.

Table 1. Summary of the glass transition temperature T_g, the melting temperature T_m, and the temperature at 5% weight loss T_{d5} with and without added LiTFSI ([Li^+]:[EO] 1:10) for **polymer A400 - 2000** as well as the **precursor A**.

Entry	EO units*	T_g [°C]	T_m [°C]	$T_{g\ +\ LiTFSI}$ [°C]	$T_{m\ +\ LiTFSI}$ [°C]	T_{d5} [°C]	$T_{d5\ +\ LiTFSI}$ [°C]
Precursor A	-	5	n.e.	n.d.	n.d.	190	n.d.
Polymer A400	11.3	-66	-1	-35	n.v.	350	320
Polymer A550	15.8	-67	14	-41	n.v.	336	306
Polymer A750	19.8	-65	27	-40	n.v.	356	328
Polymer A1000	24.3	n.v.	34	-41	n.v.	346	286
Polymer A2000	54.0	n.v.	50	-43	n.v.	351	306

n.e. = not existent, n.d. = not determined, n.v. = not visible, *calculated by ^{1}H NMR integrals.

Generally, DSC measurements of PEO-based polymer electrolytes are of particular interest since the results are closely related to the ionic conductivity[34,35]. While the precursor **polymer A** had a *glass transition temperature* T_g of around 5 °C, the series of modified **polymers A400 - A2000** showed the usual characteristics of PEO-based materials owing to their semi-crystalline structure.[36,37] Therefore, regarding their side chain length, a T_g and/or a melting point T_m of the PEO side chains was observed. For polymers bearing shorter PEO side chains (**polymers A400 - A750**) a T_g at around – 65 °C was detected, which is in accordance with the typical temperature reported in the literature[38]. However, for longer side chain lengths (**polymers A1000 & A2000** corresponding to around 24 & 54 EO repeating units) the T_g could not be observed under the measuring conditions used, owing to their higher degree of crystallinity. Instead, prominent melting points were detected. It has to be mentioned that

although **polymers A400 - A750** showed a *glass transition temperature*, they still featured melting points owing to their semi-crystalline structure.

One key point is displayed in the fact that EO side chain length, melting point T_m and required energy per mass to melt the crystalline phases ΔH_{melt} (equals to the integral of T_m) are directly correlated. **Polymer A400** with a side chain length of around 11 EO repeating units only showed a barely visible melting point at around -1 °C. However, with increasing side chain length, the melting point shifted towards higher values while also the peak integral (ΔH_{melt}) increased (**Figure 2b, 2c**). Since ΔH_{melt} is directly correlated to the degree of crystallinity, the reduction of the latter in comparison to pure PEO (196.4 J g^{-1})[39] could be calculated (**Figure 2c**). It is remarkable that **polymer A400** showed a reduction in crystallinity of around 98%, while a reduction of around 81% was found for **polymer A550**. Interestingly, even **polymer A2000**, which contains around 54 EO repeating units, still featured a remarkable reduction in crystallinity of 48%. Overall, these results showed the successful approach of side chain architectures in order to reduce the crystallinity of such PEO-based materials by a significant degree.

Additionally, the thermal behavior of the polymer materials after mixing with LiTFSI was examined. As shown in **Table 1**, the polymer electrolytes did not show any melting point after mixing with LiTFSI in a ratio of $[Li^+]$:[EO] of 1:10. Instead, they featured a glass transition temperature that was shifted to higher temperatures in comparison to the pure materials. Both effects the reduction in crystallinity as well as the shift of the T_g are typical for blends of PEO-based materials with LiTFSI.[40] On one hand, this is caused by the so-called *quasi-ionic cross-linking,* which describes the physical linking of different PEO chains by polar interaction originating from the coordination of lithium ions, thus decreasing mobility and therefore increasing the T_g. On the other hand, the *quasi-ionic cross-linking* and the bulky $TFSI^-$ anion are suppressing crystallization of PEO chains by hindering their alignment. Generally, as reported in literature[29,41], especially short PEO side chains suffer from a huge increase in the

glass transition temperature after mixing with lithium salts, probably due to the higher number of *inter chain* cross-links in comparison to *intra chain* cross-links. Since the shortest used side chain in this work has already around 11 EO repeating units, this effect was not very prominent, but yet **polymer A400** showed a noticeable higher T_g than the longer polymer derivatives **A550 – A2000** (**Table 1**).

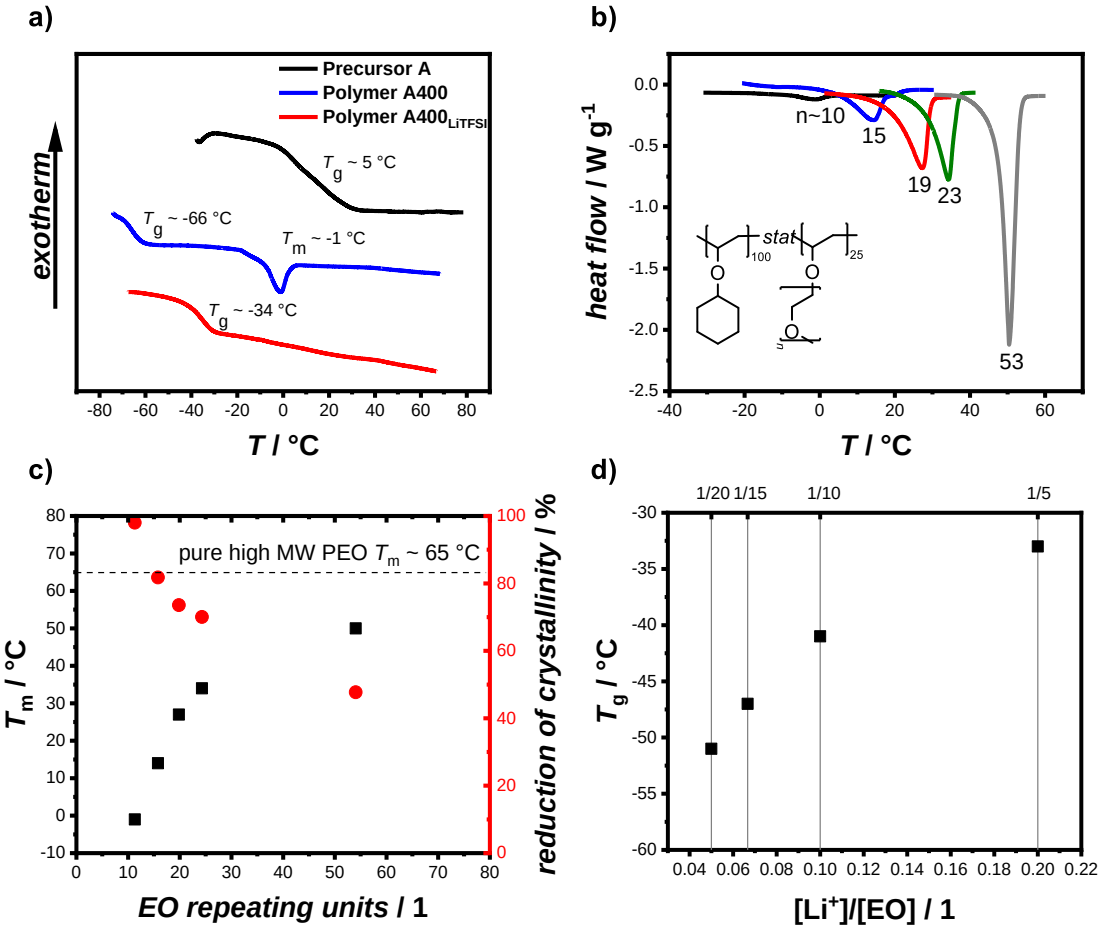

Figure 2. DSC analyses of **polymers A400 - A2000**. **a)** Showing exemplarily the difference in the thermal behavior before the attachment of PEO side chains, after the attachment and after blending with LiTFSI ([Li^+]:[EO] 1:10). **b)** Depiction of the increasing value as well as the area of the melting points T_m of the polymers bearing different PEO side chain lengths. **c)** Development of the melting points with increasing side chain length and corresponding percental reduction of crystallinity in comparison to pure PEO. (see also **Table S3**) **d)** Dependency of the glass transition temperature T_g of **polymer A1000** regarding different [Li^+]:[EO] ratios. The nearly linear trend can be explained by the direct correlation of lithium ions and *quasi-ionic cross-linking* points.

Furthermore, **polymer A1000** (average-length PEO side chain within **polymer** series **A**) was chosen to be candidate presenting the influence of LiTFSI concentration onto the *glass transition temperature (***Figure 2d***)*. Four different blends employing [Li^+]:[EO] ratios of 1:5, 1:10, 1:15 and 1:20 were prepared and DSC measurements were conducted. All four ratios were sufficient in completely suppressing the crystallization of PEO side chains, while the corresponding T_g increased nearly linearly with increasing LiTFSI concentration from -51 °C ([Li^+]:[EO] = 1:20) up to -33 °C ([Li^+]:[EO] = 1:5). This can be explained by the fact that the number of *quasi-ionic cross-linking* points increases with each added lithium ion up to a saturation limit where each oxygen atom already coordinates to one Li^+ ion.

3.3 Ionic Conductivity

Temperature dependent *electrochemical impedance spectroscopy (EIS)* was conducted to elucidate the impact of the PEO side chain length and the LiTFSI salt content on the ionic conductivity. In this regard each **Polymer A400 - A2000** was used to obtain four different polymer electrolytes featuring [Li^+]:[EO] ratios of 1:5, 1:10, 1:15 and 1:20, respectively. All ionic conductivity plots comprising all different LiTFSI ratios are shown in **Figure 3**.

As generally known for PEO-based polymer electrolytes, a strong dependency of the LiTFSI content on the ionic conductivity was observed, reflecting trends that were already discussed for the evaluation of the DSC data. As shown in **Figure 2d**, high contents of Li^+ ions lead to a high number of *quasi-ionic cross-linking* points and thus making the side chains immobile resulting in a high T_g. However, low T_g values are generally preferred, since segmental motion of PEO chains significantly assist ion transport in such materials and thus T_g can be used to have an indicator of the (side) chain mobility.[42,43] In addition, very high amounts of Li^+ ions hinder ion transport *via inter*/*intra-chain hopping*[18,44] since most oxygen atoms are already occupied thus limiting the free volume. As a result, the ionic conductivity employing a LiTFSI

content of [Li^+]:[EO] of 1:5 was the worst for all polymers studied in comparison to their mixtures featuring lower LiTFSI contents, respectively (**Figure 3a-e**).

It has to be further considered that there are several parameters influencing the ionic conductivity of polymer electrolytes in different ways analogous to the influence on the thermal properties (**Table S4**). It is well known, that the $TFSI^-$ anion decreases the crystallinity as well as the T_g due to its bulky structure, thus acting as plasticizer and therefore having a positive impact on the ionic conductivity.[45] However, since LiTFSI is introduced as a salt, the number of Li^+ ions is equivalent to the number of $TFSI^-$ anions and since the Li^+ ions drastically increase the T_g (*quasi-ionic cross-linking*), the total amount of LiTFSI has to be adjusted carefully. Furthermore, longer PEO side chain lengths increase the crystallinity as result of chain alignment in the pure polymer, but also decrease the T_g showing higher side chain mobility as discussed previously for the DSC data (**Table 1** and **Figure 2**).

The combined effects of these different parameters acting together are reflected in the ionic conductivity behavior. **Polymer A400 - A1000** (i.e. polymers with a side chain length of up to 24 EO repeating units) exhibited the highest ionic conductivity with a low amount of LiTFSI of 1:20 in comparison to higher amounts, since the crystallinity was already drastically reduced by the side chain architecture and the drawback of using more Li^+ ions was higher than the positive influence of the $TFSI^-$ anion (**Figure 3a-d**). Opposite to this, **polymer A2000** bearing the longest PEO side chain showed that the ionic conductivity at [Li^+]:[EO] of 1:20 suffered from a significant drop below 40 °C due to a beginning partial crystallization (**Figure 3e**). Since the increasing side chain length also increased the chain alignment and therefore crystallinity, a higher LiTFSI content of 1:15 was beneficial, because of the vanished crystallinity by the additional $TFSI^-$ anions. This general trend is summarized in **Table S4**Fehler! Verweisquelle konnte nicht gefunden werden..

When comparing the highest obtained ionic conductivity for **polymer A400 - A1000**, longer side chains perform better (24 > 20 > 16 > 11 units) at all measured temperatures as indicated

in **Figure 3f** and more precisely in **Figure 4**. However, when comparing **polymer A1000** (24 units) with **polymer A2000** (54 units), it is noticeable that a tradeoff between the ionic conductivity at higher and lower temperatures is established. While the longer side chain (54 units) showed a higher ionic conductivity at higher temperatures (30 °C and above) the shorter side chain (24 units) resulted in superior ionic conductivity at lower temperatures (20 °C and below). This effect can be explained by the previously described circumstances that the suppression of crystallization and the influence on the T_g cannot be addressed individually. Therefore, polymers with shorter side chains show a well suppressed chain alignment enabling superior ionic conductivity at lower temperatures but the disadvantage regarding their T_g and thus their low side chain mobility results in lower ionic conductivities at higher temperatures, where suppression of chain alignment does not play any role, while polymers with longer side chains show a lower T_g (higher side chain mobility) and thus featuring higher ionic conductivity at higher temperatures, but their lack in suppression of chain alignment results in comparable lower ionic conductivities at lower temperatures.

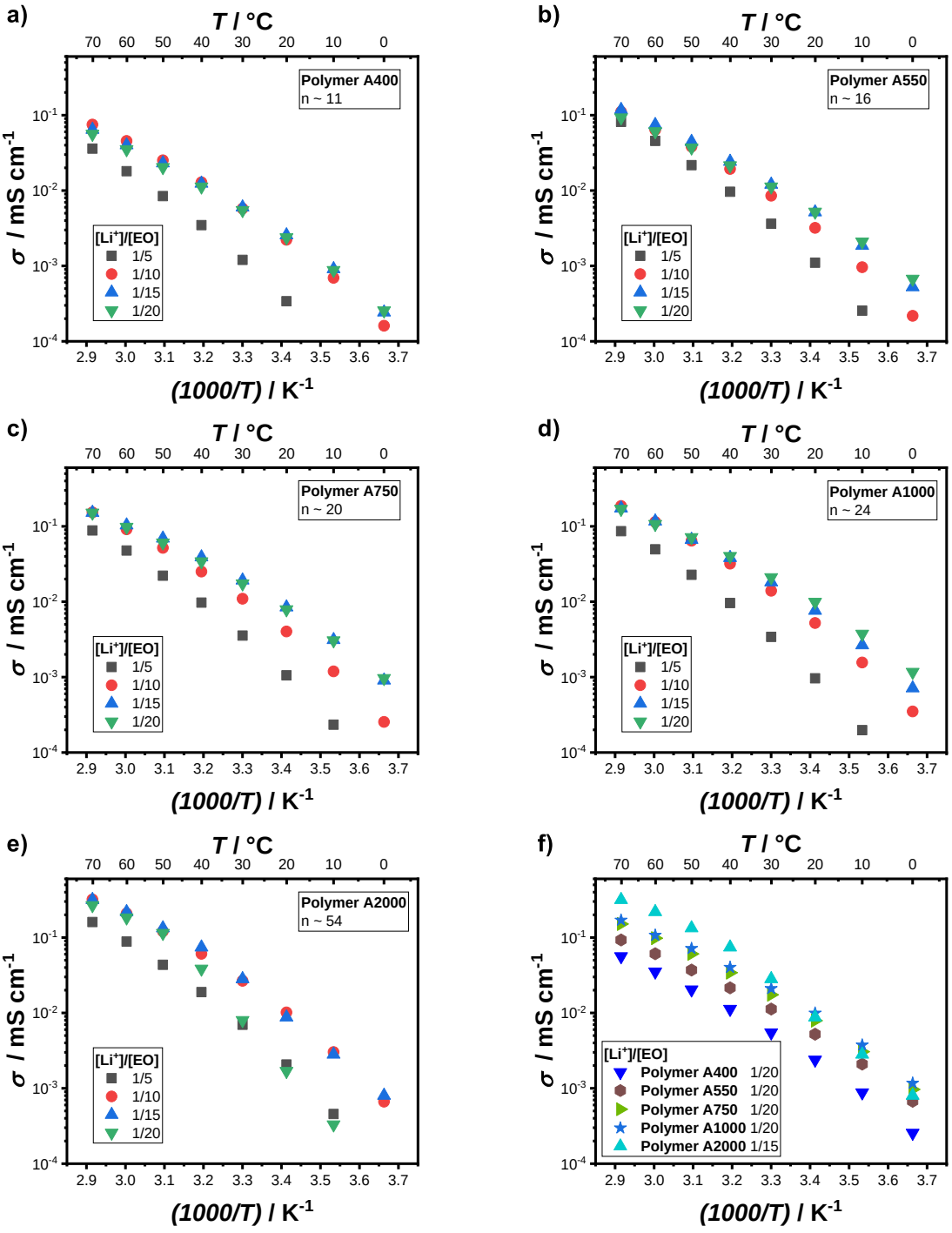

Figure 3. a) - e) Temperature dependent ionic conductivity derived from EIS measurements of the different copolymer systems bearing different PEO side chain lengths. LiTFSI content was varied in respect to EO units. **f)** Depiction of the best performing polymer:LiTFSI combinations (1:20 for **polymer A400 - A1000** and 1:15 for **polymer A2000**).

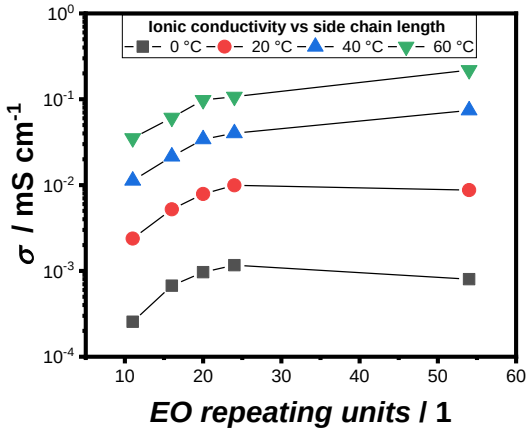

Figure 4. Depiction of the ionic conductivity in respect to EO side chain length for the different **polymers A400 - A2000**. The best performing [LiTFSI]:[EO] ratio taken from **Figure 3f** is displayed. It is notable that up to 24 repeating units a longer side chain is preferable at each measured temperature. This changes in the transition from 24 to 54 repeating units. At 30 °C and higher the longer side chain shows the higher ionic conductivity, while at temperatures below 30 °C the shorter side chain shows higher ionic conductivity.

3.4 Influence of the Grafting Density

Furthermore, the influence of the grafting density of the PEO side chains on the ionic conductivity was examined. Therefore, comparable statistical copolymers with a grafting density of 50% (**polymer** series **B**; **Figure 5a, Table S2**) in comparison to 20% for **polymer A400 - A2000** were synthesized. While doing so, we focused on the shortest (~ 11 EO units) and the longest side chains (24 and 54 EO units) as wells as [Li^+]:[EO] ratios of 1:15 and 1:20 for the *EIS* measurements as a consequence of the previously discussed results.

When comparing the DSC results of **polymer** series **B** (**Table 2**) with series **A** (**Table 1**), it became obvious that a higher grafting density resulted in a higher melting point (10, 5 and 3 °C increase for **polymer B400**, **B1000** and **B2000**, respectively) going hand in hand with a higher degree of crystallinity (**Table S3**). Still, **polymer B400**, **B1000** and **B2000** featured remarkable reductions in crystallinity of 75, 51 and 39% in comparison to pure PEO, respectively (**Figure 5b**). However, at the same time the T_g of polymers **B400**, **B1000** and **B2000** after mixing with LiTFSI was noticeable lower for each polymer (**Table 2**) in comparison to their counterparts

featuring lower grafting densities (**Table 1**). Furthermore, different amounts of LiTFSI were mixed with **polymer B1000** analogously to its counterpart **polymer A1000** revealing a lower T_g for each composition (**Figure 5c**). All these phenomena are direct results of the higher grafting density. Since there are more chains present and the distance between the chains is smaller in polymers with higher grafting densities, it is easier for them to crystallize. On the other side, there are also more side chains per main chain, resulting in smaller number of chains taking part in the *inter chain quasi-ionic cross-linking* by Li^+ ions and thus lowering T_g.

Table 2. Overview of the 3 different synthesized copolymers featuring a grafting density of 50%. T_g and T_m was obtained by DSC measurements. Samples with added LiTFSI featured a $[Li^+]$:[EO] ratio of 1:10.

Entry	EO units*	T_g [°C]	T_m [°C]	$T_{g\ +\ LiTFSI}$ [°C]	$T_{m\ +\ LiTFSI}$ [°C]
Polymer B400	11.7	n.v.	9	-42	n.v.
Polymer B1000	25.2	n.v.	39	-42	n.v.
Polymer B2000	52.2	n.v.	53	-44	n.v.

*Calculated by ^{1}H NMR integrals (difference to **polymer** series **A** within the error), n.v. = not visible.

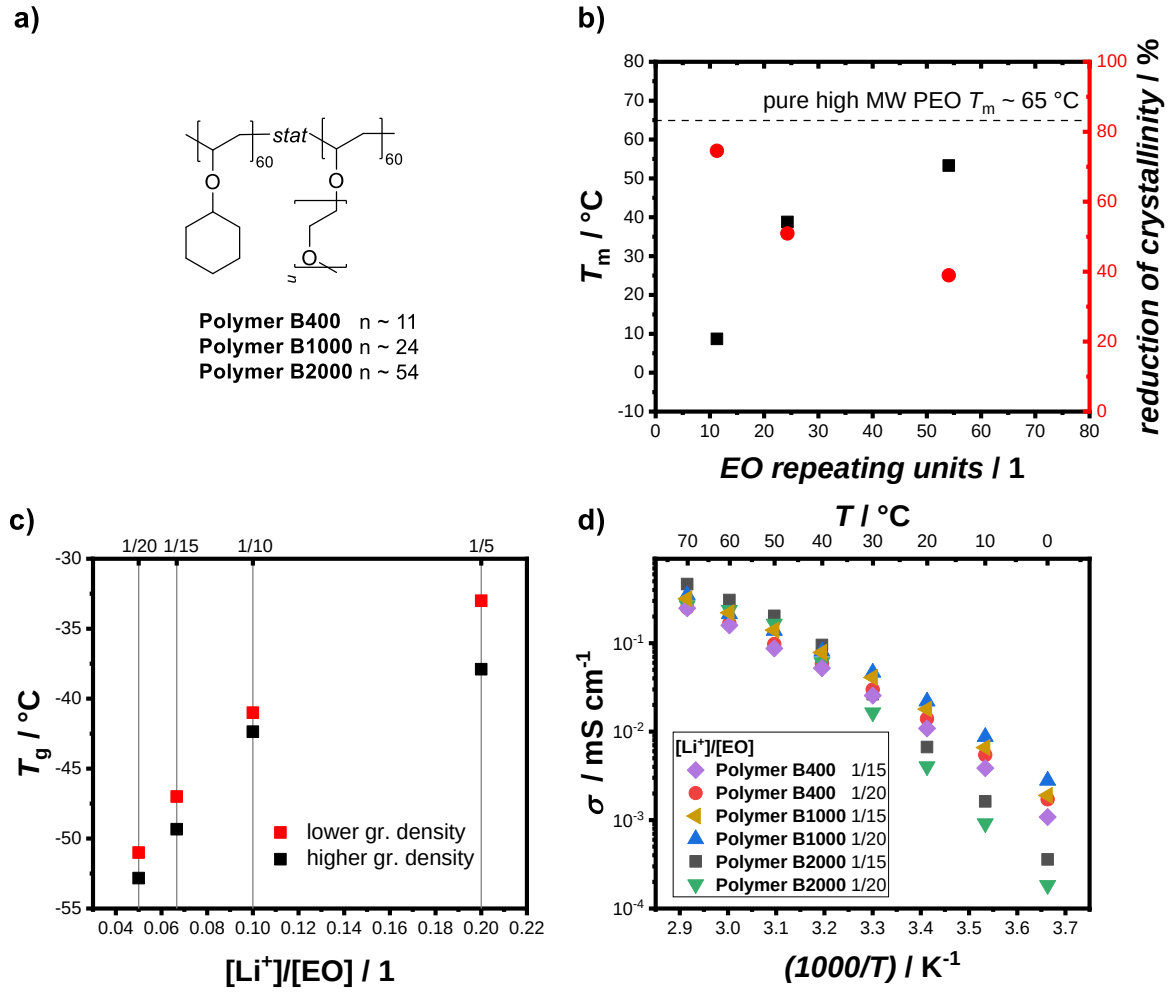

Figure 5. a) Three statistical copolymers **(polymer B400 - B2000**) were synthesized featuring a higher grafting density (monomer ratio 1:1; grafting density 50%) in comparison to **polymer A400 - A2000** (monomer ratio 4:1; grafting density 20%). **b)** Development of the melting points of **polymer B400 - B2000** with increasing side chain length and corresponding percental reduction of crystallinity in comparison to pure PEO. (see also **Table S3**) **c)** Dependency of the glass transition temperature T_g of **polymer B1000** in regard to different [Li^+]:[EO] ratios. As comparison the T_g of **polymer A1000** (see also **Figure 2d**), which features the same side chain length but lower grafting density, is shown. **d)** Temperature dependent ionic conductivity derived from EIS measurements of **polymer B400 - B2000** comprising [Li^+]:[EO] ratios of 1:15 and 1:20.

As already stated for the discussion of the ionic conductivities of **polymers A400 - A2000**, the DSC results of **polymers B400 - B2000** are in line with the results of the *EIS* measurements (**Figure 5d**, **Figure 6** and **Table 3**). Although, the initial suppression of crystallization by the side chain architecture was worse for copolymers featuring a higher grafting density in comparison to the copolymers featuring a lower grafting density (**Table 3**), it was still sufficient to eliminate crystallization in combination with added LiTFSI for **polymer B400** and **B1000**

(11 and 24 EO repeating units). At the same time, there was an improvement regarding the T_g resulting in higher chain mobility and thus in higher ionic conductivities at all measured temperatures in comparison to **polymer A400** and **A1000**, respectively (**Figure 6** and **Table 3**). For **polymer B2000** the trend of a temperature-dependent tradeoff, which was already observed for its counterpart **polymer A2000,** continued. Here, the higher grafting density resulted once more in a reduced suppression of chain alignment but a slightly lower T_g, which consequently established an even bigger tradeoff between higher and lower temperatures (**Figure 6** and **Table 3**). When summarizing these findings, it can be stated that an increasing grafting density results in the same effect as increasing side chain length.

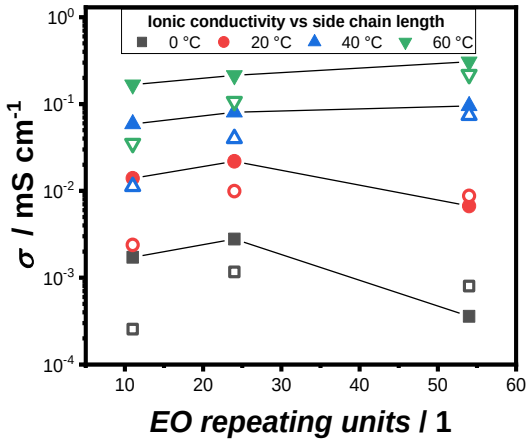

Figure 6. Depiction of the ionic conductivity in respect to EO side chain length for the different **polymers B400 - B2000** (—■—). The best performing [LiTFSI]:[EO] ratio taken from **Figure 5d** is displayed (**B400** & **B1000**: [Li]:[EO] 1:20; **B2000**: [Li]:[EO] 1:20) . As comparison the ionic conductivity of **polymer A400**, **A1000** and **A2000** (□) taken from **Figure 4** is shown.

Table 3. Summarizing comparison of the reduction of the crystallinity (**RC**) of the copolymers in comparison to pure PEO, the T_g ([Li^+]:[EO] ratio 1:10) of the polymer electrolyte and the ionic conductivity at 0 as wells as 60 °C.

Entry	RC [%]	$T_{g\ +\ LiTFSI}$ [°C]	$\sigma_{0°C}$* [mS cm^{-1}]	$\sigma_{60°C}$* [mS cm^{-1}]
Polymer A400	98	-35	$0.26 \cdot 10^{-3}$	$0.35 \cdot 10^{-2}$
Polymer B400	75	-42	$1.72 \cdot 10^{-3}$	$1.67 \cdot 10^{-1}$

Polymer A1000	70	-41	$1.17 \cdot 10^{-3}$	$1.07 \cdot 10^{-1}$
Polymer B1000	50	-42	$2.79 \cdot 10^{-3}$	$2.14 \cdot 10^{-1}$
Polymer A2000	48	-43	$0.80 \cdot 10^{-3}$	$2.19 \cdot 10^{-1}$
Polymer B2000	39	-44	$0.36 \cdot 10^{-3}$	$3.07 \cdot 10^{-1}$

***** taken from **Figure 6**

4. Conclusion

A series of different vinyl ether-based PEO side chain copolymers was synthesized and the corresponding polymer electrolytes featuring different PEO side chain lengths, different grafting densities and varying LiTFSI salt contents were studied. Consequently, a detailed picture of the influence of these different parameters onto the thermal behavior and the ionic conductivity was drawn. Herein, we were able to show that the PEO side chain approach is capable of reducing the degree of crystallinity of PEO phases dramatically, ranging from a reduction by 98% (**polymer A400**) to 39% (**polymer B2000**) in comparison to pure PEO. Furthermore, we described precisely that copolymers bearing longer PEO side chains and higher grafting densities showed higher crystallization tendencies but lower T_gs. Also, the addition of LiTFSI reduced the crystallization due to the $TFSI^-$ anion acting as plasticizer, while the Li^+ cations increased the T_g as a result of *quasi-ionic cross-linking* of PEO chains. When summing up all these effects, it is obvious that each parameter has positive and negative influences onto the thermal behavior. Since this is directly reflected in the ionic conductivity, a 'sweet spot' has to be found in order to minimize chain alignment, while at the same time maintaining a low T_g. However, this seems only to be partially possible, because at one point a tradeoff between high and low temperature ionic conductivity is established. Consequently, the best achieved ionic conductivity at room temperature (20 °C) was $2.19 \cdot 10^{-2}$ mS cm^{-1}

comprising **polymer B1000** (50% grafting density, 24 units side chain) and a [LiTFSI]:[EO] ratio of 1:20, while at 60 °C **polymer B2000 (**50% grafting density, 54 units side chain) showed the best results ($3.07 \bullet 10^{-1}$ mS cm^{-1}) when employing a [LiTFSI]:[EO] ratio of 1:15. Overall, we could provide a fundamental and detailed view of the strong relationship between structure and ionic conductivity, thus acting as guidance for future studies on PEO-based side chain architectures for application as solid polymer electrolytes.

ASSOCIATED CONTENT

Supporting Information

The Supporting Information is available free of charge. NMR spectra, synthesis details, SEC data, TGA graph, DSC data and calculations.

AUTHOR INFORMATION

Corresponding Author

Patrick Theato — Karlsruhe Institute of Technology, Karlsruhe, Germany, E-mail: patrick.theato@kit.edu

Authors

Andreas J. Butzelaar — Karlsruhe Institute of Technology, Karlsruhe, Germany

Kun L. Liu — Helmholtz-Institute Münster, Forschungszentrum Jülich, Münster, Germany.

Philipp Röring — Helmholtz-Institute Münster, Forschungszentrum Jülich, Münster, Germany.

Gunther Brunklaus — Helmholtz-Institute Münster, Forschungszentrum Jülich, Münster, Germany; University of Münster, Münster, Germany.

Martin Winter — Helmholtz-Institute Münster, Forschungszentrum Jülich, Münster, Germany; University of Münster, Münster, Germany.

ACKNOWLEDGMENT

Financial support from the German Federal Ministry of Education and Research (BMBF) within 'FestBatt' (13XP0175A) is gratefully acknowledged.

References

(1) Blomgren, G. E. The Development and Future of Lithium Ion Batteries. *J. Electrochem. Soc.* **2017**, *164* (1), A5019-A5025. DOI: 10.1149/2.0251701jes.

(2) Nitta, N.; Wu, F.; Lee, J. T.; Yushin, G. Li-ion battery materials: present and future. *Materials Today* **2015**, *18* (5), 252–264. DOI: 10.1016/j.mattod.2014.10.040.

(3) Tarascon, J. M.; Armand, M. Issues and challenges facing rechargeable lithium batteries. *Nature* **2001**, *414* (6861), 359–367. DOI: 10.1038/35104644.

(4) Hammami, A.; Raymond, N.; Armand, M. Lithium-ion batteries: runaway risk of forming toxic compounds. *Nature* **2003**, *424* (6949), 635–636. DOI: 10.1038/424635b.

(5) Goodenough, J. B.; Kim, Y. Challenges for Rechargeable Li Batteries †. *Chem. Mater.* **2010**, *22* (3), 587–603. DOI: 10.1021/cm901452z.

(6) Zheng, F.; Kotobuki, M.; Song, S.; Lai, M. O.; Lu, L. Review on solid electrolytes for all-solid-state lithium-ion batteries. *Journal of Power Sources* **2018**, *389*, 198–213. DOI: 10.1016/j.jpowsour.2018.04.022.

(7) Aziz, S. B.; Woo, T. J.; Kadir, M.F.Z.; Ahmed, H. M. A conceptual review on polymer electrolytes and ion transport models. *Journal of Science: Advanced Materials and Devices* **2018**, *3* (1), 1–17. DOI: 10.1016/j.jsamd.2018.01.002.

(8) Devaux, D.; Bouchet, R.; Glé, D.; Denoyel, R. Mechanism of ion transport in PEO/LiTFSI complexes: Effect of temperature, molecular weight and end groups. *Solid State Ionics* **2012**, *227*, 119–127. DOI: 10.1016/j.ssi.2012.09.020.

(9) Karmakar, A.; Ghosh, A. A comparison of ion transport in different polyethylene oxide–lithium salt composite electrolytes. *Journal of Applied Physics* **2010**, *107* (10), 104113. DOI: 10.1063/1.3428389.

(10) Mindemark, J.; Lacey, M. J.; Bowden, T.; Brandell, D. Beyond PEO—Alternative host materials for Li + -conducting solid polymer electrolytes. *Progress in Polymer Science* **2018**, *81*, 114–143. DOI: 10.1016/j.progpolymsci.2017.12.004.

(11) Krause, C. H.; Butzelaar, A. J.; Diddens, D.; Dong, D.; Théato, P.; Bedrov, D.; Hwang, B.-J.; Winter, M.; Brunklaus, G. Quasi-solid single ion conducting polymer electrolyte membrane containing novel fluorinated poly(arylene ether sulfonimide) for lithium metal batteries. *Journal of Power Sources* **2021**, *484*, 229267. DOI: 10.1016/j.jpowsour.2020.229267.

(12) Krause, C. H.; Röring, P.; Onishi, H.; Diddens, D.; Thienenkamp, J. H.; Brunklaus, G.; Winter, M.; Cekic-Laskovic, I. Propylene carbonate-nitrile solvent blends for thermally stable gel polymer lithium ion battery electrolytes. *Journal of Power Sources* **2020**, *478*, 229047. DOI: 10.1016/j.jpowsour.2020.229047.

(13) Wright, P. V. Electrical conductivity in ionic complexes of poly(ethylene oxide). *Brit. Poly. J.* **1975**, *7* (5), 319–327. DOI: 10.1002/pi.4980070505.

(14) Magistris, A.; Singh, K. PEO-based polymer electrolytes. *Polym. Int.* **1992**, *28* (4), 277–280. DOI: 10.1002/pi.4990280406.

(15) Fenton, D. E.; Parker, J. M.; Wright, P. V. Complexes of alkali metal ions with poly(ethylene oxide). *Polymer* **1973**, *14* (11), 589. DOI: 10.1016/0032-3861(73)90146-8.

(16) Homann, G.; Stolz, L.; Nair, J.; Laskovic, I. C.; Winter, M.; Kasnatscheew, J. Poly(Ethylene Oxide)-based Electrolyte for Solid-State-Lithium-Batteries with High Voltage Positive Electrodes: Evaluating the Role of Electrolyte Oxidation in Rapid Cell Failure. *Scientific Reports* **2020**, *10* (1), 4390. DOI: 10.1038/s41598-020-61373-9.

(17) Homann, G.; Stolz, L.; Winter, M.; Kasnatscheew, J. Elimination of "Voltage Noise" of Poly (Ethylene Oxide)-Based Solid Electrolytes in High-Voltage Lithium Batteries: Linear versus Network Polymers. *iScience* **2020**, *23* (6), 101225. DOI: 10.1016/j.isci.2020.101225.

(18) Xue, Z.; He, D.; Xie, X. Poly(ethylene oxide)-based electrolytes for lithium-ion batteries. *J. Mater. Chem. A* **2015**, *3* (38), 19218–19253. DOI: 10.1039/C5TA03471J.

(19) *Batteries LMP® | Blue Solutions*. https://www.blue-solutions.com/en/blue-solutions/technology/batteries-lmp/ (accessed 2020-12-09).

(20) Osada, I.; Vries, H. de; Scrosati, B.; Passerini, S. Ionic-Liquid-Based Polymer Electrolytes for Battery Applications. *Angewandte Chemie (International ed. in English)* **2016**, *55* (2), 500–513. DOI: 10.1002/anie.201504971.

(21) Sun, C.; Liu, J.; Gong, Y.; Wilkinson, D. P.; Zhang, J. Recent advances in all-solid-state rechargeable lithium batteries. *Nano Energy* **2017**, *33*, 363–386. DOI: 10.1016/j.nanoen.2017.01.028.

(22) Bandara, L.R.A.K.; Dissanayake, M.A.K.L.; Mellander, B.-E. Ionic conductivity of plasticized(PEO)-LiCF3SO3 electrolytes. *Electrochimica Acta* **1998**, *43* (10-11), 1447–1451. DOI: 10.1016/S0013-4686(97)10082-2.

(23) Nicotera, I. A study of stability of plasticized PEO electrolytes. *Solid State Ionics* **2002**, *146* (1-2), 143–150. DOI: 10.1016/S0167-2738(01)01003-7.

(24) Fergus, J. W. Ceramic and polymeric solid electrolytes for lithium-ion batteries. *Journal of Power Sources* **2010**, *195* (15), 4554–4569. DOI: 10.1016/j.jpowsour.2010.01.076.

(25) Wen, Z. Blend-based polymer electrolytes of poly(ethylene oxide) and hyperbranched poly[bis(triethylene glycol)benzoate] with terminal acetyl groups. *Solid State Ionics* **2000**, *134* (3-4), 281–289. DOI: 10.1016/S0167-2738(00)00707-4.

(26) Wright, P. V. Polymer electrolytes—the early days. *Electrochimica Acta* **1998**, *43* (10-11), 1137–1143. DOI: 10.1016/S0013-4686(97)10011-1.

(27) Paranjape, N.; Mandadapu, P. C.; Wu, G.; Lin, H. Highly-branched cross-linked poly(ethylene oxide) with enhanced ionic conductivity. *Polymer* **2017**, *111*, 1–8. DOI: 10.1016/j.polymer.2017.01.014.

(28) Rolland, J.; Brassinne, J.; Bourgeois, J.-P.; Poggi, E.; Vlad, A.; Gohy, J.-F. Chemically anchored liquid-PEO based block copolymer electrolytes for solid-state lithium-ion batteries. *J. Mater. Chem. A* **2014**, *2* (30), 11839–11846. DOI: 10.1039/C4TA02327G.

(29) Itoh, T.; Fujita, K.; Uno, T.; Kubo, M. Polymer electrolytes based on vinyl ethers with various EO chain length and their polymer electrolytes cross-linked by electron beam irradiation. *Ionics* **2017**, *23* (2), 257–264. DOI: 10.1007/s11581-016-1815-x.

(30) Aoshima, S.; Higashimura, T. Living cationic polymerization of vinyl monomers by organoaluminum halides. 3. Living polymerization of isobutyl vinyl ether by

ethyldichloroaluminum in the presence of ester additives. *Macromolecules* **1989**, *22* (3), 1009–1013. DOI: 10.1021/ma00193a001.

(31) Gao, H.; Matyjaszewski, K. Synthesis of molecular brushes by "grafting onto" method: combination of ATRP and click reactions. *Journal of the American Chemical Society* **2007**, *129* (20), 6633–6639. DOI: 10.1021/ja0711617.

(32) Aoshima, S.; Onishi, H.; Kamiya, M.; Shachi, K.; Kobayashi, E. Role of added Lewis base and alkylaluminum halide on living cationic polymerization of vinyl ether. *J. Polym. Sci. A Polym. Chem.* **1994**, *32* (5), 879–887. DOI: 10.1002/pola.1994.080320509.

(33) Kerner, M.; Plylahan, N.; Scheers, J.; Johansson, P. Ionic liquid based lithium battery electrolytes: fundamental benefits of utilising both TFSI and FSI anions? *Physical chemistry chemical physics : PCCP* **2015**, *17* (29), 19569–19581. DOI: 10.1039/c5cp01891a.

(34) Lehmann, M. L.; Yang, G.; Nanda, J.; Saito, T. Well-designed Crosslinked Polymer Electrolyte Enables High Ionic Conductivity and Enhanced Salt Solvation. *J. Electrochem. Soc.* **2020**, *167* (7), 70539. DOI: 10.1149/1945-7111/ab7c6e.

(35) Kim, Y. W.; Lee, W.; Choi, B. K. Relation between glass transition and melting of PEO–salt complexes. *Electrochimica Acta* **2000**, *45* (8-9), 1473–1477. DOI: 10.1016/S0013-4686(99)00362-X.

(36) Ibrahim, S.; Yasin, S. M. M.; Ahmad, R.; Johan, M. R. Conductivity, thermal and morphology studies of PEO based salted polymer electrolytes. *Solid State Sciences* **2012**, *14* (8), 1111–1116. DOI: 10.1016/j.solidstatesciences.2012.05.019.

(37) Chowdari, B.; Huq, R.; Farrington, G. Thermal and electrical characterization of PEO-based polymer electrolytes containing mixed Co(II) and Li(I)☆. *Solid State Ionics* **1992**, *57* (1-2), 49–58. DOI: 10.1016/0167-2738(92)90063-U.

(38) Stolwijk, N. A.; Heddier, C.; Reschke, M.; Wiencierz, M.; Bokeloh, J.; Wilde, G. Salt-Concentration Dependence of the Glass Transition Temperature in PEO–NaI and PEO–LiTFSI Polymer Electrolytes. *Macromolecules* **2013**, *46* (21), 8580–8588. DOI: 10.1021/ma401686r.

(39) Dreezen, G.; Koch, M.H.J.; Reynaers, H.; Groeninckx, G. Miscible binary blends of poly(ethylene oxide) and an amorphous aromatic polyamide (Aramide 34I): crystallization, melting behavior and semi-crystalline morphology. *Polymer* **1999**, *40* (23), 6451–6463. DOI: 10.1016/S0032-3861(98)00849-0.

(40) Gorecki, W.; Jeannin, M.; Belorizky, E.; Roux, C.; Armand, M. Physical properties of solid polymer electrolyte PEO(LiTFSI) complexes. *J. Phys.: Condens. Matter* **1995**, *7* (34), 6823–6832. DOI: 10.1088/0953-8984/7/34/007.

(41) Itoh, T.; Fujita, K.; Inoue, K.; Iwama, H.; Kondoh, K.; Uno, T.; Kubo, M. Solid polymer electrolytes based on alternating copolymers of vinyl ethers with methoxy oligo(ethyleneoxy)ethyl groups and vinylene carbonate. *Electrochimica Acta* **2013**, *112*, 221–229. DOI: 10.1016/j.electacta.2013.08.124.

(42) Brooks, D. J.; Merinov, B. V.; Goddard, W. A.; Kozinsky, B.; Mailoa, J. Atomistic Description of Ionic Diffusion in PEO–LiTFSI: Effect of Temperature, Molecular Weight, and Ionic Concentration. *Macromolecules* **2018**, *51* (21), 8987–8995. DOI: 10.1021/acs.macromol.8b01753.

(43) Chen, X. C.; Sacci, R. L.; Osti, N. C.; Tyagi, M.; Wang, Y.; Palmer, M. J.; Dudney, N. J. Study of segmental dynamics and ion transport in polymer–ceramic composite electrolytes by quasi-elastic neutron scattering. *Mol. Syst. Des. Eng.* **2019**, *4* (2), 379–385. DOI: 10.1039/C8ME00113H.

(44) Bresser, D.; Lyonnard, S.; Iojoiu, C.; Picard, L.; Passerini, S. Decoupling segmental relaxation and ionic conductivity for lithium-ion polymer electrolytes. *Mol. Syst. Des. Eng.* **2019**, *4* (4), 779–792. DOI: 10.1039/C9ME00038K.

(45) Shin, J. Ionic liquids to the rescue? Overcoming the ionic conductivity limitations of polymer electrolytes. *Electrochemistry Communications* **2003**, *5* (12), 1016–1020. DOI: 10.1016/j.elecom.2003.09.017.

Table of Contents Artwork